MOF–stabilized perfluorinated palladium cages catalyze the additive–free aerobic oxidation of aliphatic alcohols to acids

Dr. Rossella Greco,[a] Estefania Tiburcio–Fortes,[b] Dr. Antonio Fernandez,[c] Dr. Carlo Marini,[d] Dr. Alejandro Vidal–Moya,[a] Dr. Judit Oliver–Meseguer,[a] Prof. Donatella Armentano,*[e] Prof. Emilio Pardo,*[b] Dr. Jesús Ferrando–Soria,*[b] and Dr. Antonio Leyva–Pérez.*[a]

Abstract: Extremely high electrophilic metal complexes, composed by a metal cation and very electron poor σ–donor ancillary ligands, are expected to be privileged catalysts for oxidation reactions in organic chemistry. However, their low lifetime prevents any use in catalysis. Here we show the synthesis of fluorinated pyridine–Pd^{2+} coordinate cages within the channels of an anionic tridimensional metal organic framework (MOF), and their use as efficient metal catalysts for the aerobic oxidation of aliphatic alcohols to carboxylic acids without any additive. Mechanistic studies strongly support that the MOF–stabilized coordination cage with perfluorinated ligands unleashes the full electrophilic potential of Pd^{2+} to dehydrogenate primary alcohols, without any base, and also to activate O_2 for the radical oxidation to the aldehyde intermediate. This study opens the door to design catalytic perfluorinated complexes for challenging organic transformations, where an extremely high electrophilic metal site is required.

Introduction

Catalytic metal complexes with ancillary ligands –*i.e.* ligands that do not participate directly in the reaction, but keep the metal complex structurally operative– are paramount in organic synthesis. Aromatic C–H activation[1–3] and oxidation reactions[4] are usually catalyzed by electrophilic metal complexes where the ancillary ligand does not deplete much cationic charge from the metal site. However, a balance between metal complex lifetime and metal Lewis acidity is particularly difficult to achieve for sigma (σ) donor ancillary ligands. Figure 1a shows that, in general, the more electron donor the ligand is, the more stable the complex becomes, but at expenses of decreasing the metal Lewis acidity/catalytic activity. This dichotomy has been often overcome with different chemical manifolds; such as oxidizing the ligand[5] or the metal to a high–valence state,[6,7] and using non–coordinating counteranions or other donor–acceptor ligands, with anchimeric assistance or redox properties.[8–18] However, these approaches eventually increase the synthetic complexity and price of the final metal catalyst.

A straightforward synthetic strategy to decrease the electronic donation of the ligand to the metal is fluorination of the former, due to the strong inductive effect of fluoride.[19] Indeed, monofluorinated pyridine–Pd^{2+} complexes have been reported as extremely active catalysts for carbon–carbon cross–coupling reactions and oxidation reactions after aryl C–H activation.[20] On this basis, it is reasonable to think that perfluorinated pyridines will give even better results,[21] since are weaker electron σ–donor ligands, and consequently, they will increase more the electrophilicity of the metal catalyst, as shown in Figure 1b. Moreover, perfluoropyridines are one order of magnitude cheaper than the corresponding mono– and bis–fluorinated pyridines[22–26] –since pyridine fluorination is difficult to stop at one carbon and goes all through to the perfluorinated derivative skeleton. However, despite both suitable features, perfluorinated pyridines have not been profited in catalysis, as consequence of their inability to bind strongly enough metal cations and stabilize the resulting complex. Thus, it is difficult to find any literature example of a catalytically efficient perfluorinated pyridine complex, despite all the precedents suggest that, if conveniently formed and stabilized, they may show an enhanced catalytic activity respect less fluorinated derivatives for selected organic reactions.[27,28]

Figure 1c shows that highly electrophilic complexes would be relevant for the aerobic oxidation of aliphatic alcohols to the corresponding carboxylic acids. Aliphatic alcohols are challenging alcohols to be oxidized in comparison with benzylic alcohols, and this is an industrial reaction which usually requires high amount of metal catalysts, stoichiometric bases and harsh oxidants, generating polluting and dangerous waste at the end of the reaction.[29–38] Despite many metal catalytic systems have been designed,[34,37,39–41] and those based on palladium metal –including pyridine–type molecular complexes[4,42–46] and heterogeneous catalysts[47–52] have proven to be successful, they generally need of bases and/or other additives. Only electrochemical methods seem to circumvent the use of bases with high efficiency.[53] The role of the base is to deprotonate the metal–coordinated primary alcohol, since the pK_a of the resulting metal alcoholate complex is still too low for a single metal–mediated deprotonation. This is particularly true for simple alkyl alcohols, where other electron withdrawing groups are not present to assist the deprotonation –*i.e.* benzyl alcohols.[54] However, if a very electrophilic metal site could be able to activate sufficiently the primary alkyl alcohol for spontaneous dehydrogenation, the base could be suppressed,[55,56] and the corresponding aldehyde would be formed after β–hydride

[a] *Instituto de Tecnología Química (UPV–CSIC), Universidad Politècnica de València–Consejo Superior de Investigaciones Científicas, Avda. de los Naranjos s/n, 46022 Valencia, Spain. /twitter.com/CatSusGroup_ITQ*
[b] *Departamento de Química Inorgánica, Instituto de Ciencia Molecular (ICMol), Catedrático José Beltrán Martínez, 2, Universidad de Valencia, 46980 Paterna, Valencia, Spain.*
[c] *Chemistry Department, Sir David Davies Building, Loughborough University, Loughborough LE11 3TU, United Kingdom.*
[d] *CELLS−ALBA Synchrotron, E–08290 Cerdanyola del Vallès, Barcelona, Spain.*
[e] *Dipartimento di Chimica e Tecnologie Chimiche (CTC), Università della Calabria, via P. Bucci, 12, Rende 87036, Cosenza, Italy.*

Corresponding authors emails: donatella.armentano@unical.it, Emilio.Pardo@uv.es, jesus.ferrando@uv.es, anleyva@itq.upv.es. Supporting information for this article is given via a link at the end of the document. Deposition Number "https://www.ccdc.cam.ac.uk/services/structures?id=doi:10.1002/chem.202103781"> CCDC 2107391 (for **4**) contain(s) the supplementary crystallographic data for this paper. These data are provided free of charge by the joint Cambridge Crystallographic Data Centre and Fachinformationszentrum Karlsruhe http://www.ccdc.cam.ac.uk/structures ".

elimination under aerobic conditions.[57–60] In addition, as no additional nucleophiles are present in the reaction medium –nor bases, nor additives and even nor electron donor ligands– the catalytic electrophilic Pd^{2+} could be regenerated back by activating O_2 in the presence of the so–formed aldehyde, and leading to the corresponding carboxylic acid after radical scission.[61,62] Thus, *a priori*, this additive–free mechanism constitutes a very simple and efficient way to convert abundant aliphatic primary alcohols into industrially relevant fatty carboxylic acids.[63] But, to this end, we will have to find the manner to form and stabilize highly electrophilic perfluorinated pyridine complexes.

In connection with the research lines of our groups, a type of crystalline porous materials[64–70]–so–called metal–organic frameworks (MOFs)– have been recently successfully used as platforms for the *in–situ* MOF–driven formation of robust and catalytically active supramolecular coordination compounds (SCCs) within their channels (SCCs@MOFs).[71,72] In particular, previously reported palladium SCCs@MOFs[71] exhibited high structural stability under reaction conditions –due to the formation of stabilizing mechanical interactions between the SCCs and the MOF network– and improved catalytic activities and selectivities for metal–catalysed reactions –*i.e.* coupling of boronics and/or alkynes–, as consequence of the limited, but tunable, accessible void space for catalysis. On this basis, with the aim to further expand this nascent synergetic hybridization between SCCs and MOFs, we wondered if it will be possible to take advantage of the same synthetic strategy and MOFs pore´s chemistry to construct catalytically active fluorinated pyridine–type Pd^{2+} SCCs@MOFs, tentatively showing enhanced catalytic activity respect homogenous complexes in the base–free oxidation of aliphatic primary alcohols to carboxylic acids. Besides its interest from the point–of–view of developing efficient heterogenous catalyst in relevant industrial reactions, this will be also interesting from a fundamental perspective. This work represents one of the few reported examples where the confined space of the MOF is used to build up otherwise not accessible SCCs, which evidences the uniqueness of MOFs chemistry

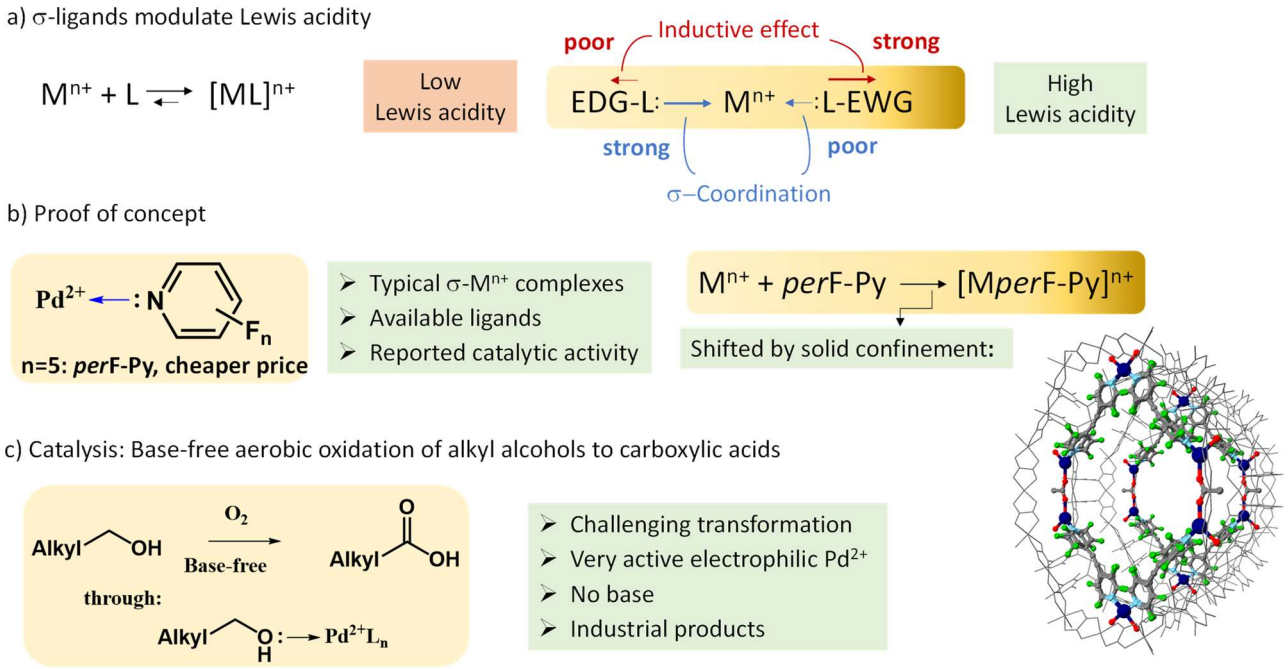

Figure 1. a) Modulation of the Lewis acidity in a metal cation by σ–coordinating ligands. Stronger ligands stabilize the metal complex but decrease Lewis acidity. b, c) Case study: catalytic perfluorinated pyridine Pd(II) complexes for the base–free aerobic oxidation of alkyl alcohols to carboxylic acids. Locking of the electrophilic σ–metal complex by formation of a coordination cage within a MOF.

Results and Discussion

Synthesis and characterization of SCCs@MOF.

We have chosen the highly crystalline MOF, of formula $[Pd^{II}(NH_3)_4][Pd^{II}_2(\mu–O)(NH_3)_6(NH_4)_2]_{0.5}\{Ni^{II}_4[Cu^{II}_2(Me_3mpba)_2]_3\} \cdot 52H_2O$ (**1**),[73] as chemical *nano*reactor for the post–synthetic construction of fluorinated pyridine–Pd^{2+} SCCs inside the MOF´s channels. Figure 2a shows its crystal structure, which features huge octagonal nano–pores (virtual diameter of *ca*. 2.0 nm) filled by Pd^{II} ions, either monomeric or self–assembled in dimers and stabilized by host–guest interactions. The crystals of **1** were soaked in an acetonitrile/water (2:1) solution of sodium acetate and different fluorinated pyridine ligands –$L_{1–3}$; L_1 = bis(3–fluoro–pyridin–4–yl)acetylene, L_2 = bis (2,3–difluoro–pyridin–4–

ykl)acetylene and L_3 = bis(2,3,5,6–tetrafluoro–pyridin–4–yl)acetylene–, prepared by Sonogashira coupling / silane deprotection of the corresponding iodides and silyl acetylenes (see Supporting Information Figure S1), to led to the formation of SCCs@MOF **2**–**4**, respectively. The characterization of **2**–**4** was performed by different characterization techniques (see ahead): inductively coupled plasma–mass spectrometry (ICP–MS), elemental, thermo–gravimetric and powder X–ray diffraction (PXRD) analyses, N_2 adsorption isotherm, X–ray photoelectron (XPS), X–ray absorption and X–ray absorption near edge structure (XANES) spectroscopies, and also solid–state magic–spinning ^{19}F nuclear magnetic resonance (SS MAS ^{19}F–NMR).

The results of this multitechnique approach could be successfully confirmed for L_3, with single crystal X–ray diffraction (SC–XRD) of **4** under synchrotron radiation, which evidenced the self–assembling of a novel supramolecular hexameric Pd^{II} square SCC within the biggest channels of **1**, to lead to a SCCs@MOF of formula $[Pd^{II}(NH_3)_4)]_{1.5}[Pd^{II}_6(\mu$–$HOAc)_2(H_2O)_{12}(L_3)_4]_{0.08333}\{Ni^{II}_4[Cu^{II}_2(Me_3mpba)_2]_3\} \cdot 28H_2O$ (**4**), as shown in Figures 2 and 3 (see also Figures S2–S7 and Table S1).

Attempts to solve the crystal structure of **2** and **3** were unsuccessful. Despite not having the security of the atomic resolution provided by SCXRD, the multi–technique approach used –commonly applied in solving highly complex architectures, when SCXRD is not possible– and the similarities of the ligands allowed us to propose tentatively formulae for **2** and **3**, $[Pd^{II}(NH_3)_4)]_{1.5}[Pd^{II}_6(\mu$–$HOAc)_2(H_2O)_{12}(L_1)_4]_{0.08333}\{Ni^{II}_4[Cu^{II}_2(Me_3mpba)_2]_3\} \cdot 25H_2O$ (**2**) $[Pd^{II}(NH_3)_4)]_{1.5}[Pd^{II}_6(\mu$–$HOAc)_2(H_2O)_{12}(L_2)_4]_{0.08333}\{Ni^{II}_4[Cu^{II}_2(Me_3mpba)_2]_3\} \cdot 26H_2O$ (**3**). Conversely for **4**, application of cutting–edge X–ray crystallography techniques, allowed us to unveil that the 3D network of the anionic $Ni^{II}_4Cu^{II}_6$ porous framework acts in response to perfluorinated pyridine ligand insertion simply with a distortion of the pores' shape, accounting for a phase transition from the tetragonal (*P*4/*mmm* space group of **1**) to orthorhombic system. Indeed, **4** crystallizes in the *Cmmm* space group, with the $[Pd^{II}_6(\mu$–$HOAc)_2(H_2O)_{12}(L_3)_4]$ cages located in the hydrophilic distorted octagonal pores [virtual diameter of *ca*. 2.2 nm] previously occupied by the Pd^{2+} dimers of **1**.

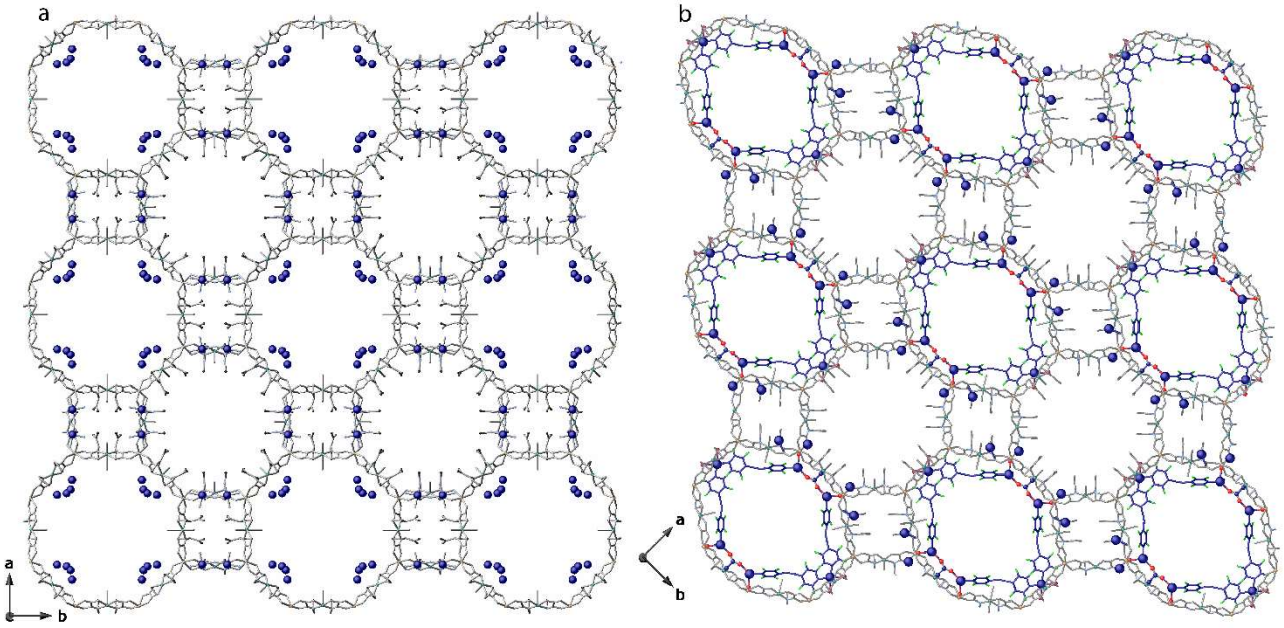

Figure 2. From MOFs 1 to 4. Comparative perspectives of the crystal structures of 1 and 4. (a) View along *c* crystallographic axis of crystal structure of the precursor **1**,[73] featuring channels filled by $[Pd^{II}(NH_3)_4][Pd^{II}_2(\mu$–$O)(NH_3)_6)(NH_4)_2]$. (b) View of the crystal structure, determined by synchrotron X–ray diffraction, of **4**, where $[Pd^{II}_6(\mu$–$HOAc)_2(H_2O)_{12}(L_3)_4]$ cages are self–assembled within the confined spaces by perfluorinated ligand L_3. Ligands atoms of the heterobimetallic $Ni^{II}_4Cu^{II}_6$ 3D anionic network are depicted as grey sticks, with cyan or orange spheres for copper and nickel metal ions, respectively. Pd(II) cations in the pores and ligands forming the cages, are represented by blue spheres and blue sticks (with fluorine in green), respectively, with oxygen atoms as red spheres.

Monomeric $\{[Pd^{II}(NH_3)_4]^{2+}/[Pd^{II}(H_2O)_x(NH_3)_{4-x}]^{2+}\}$ complexes still reside both in the square smallest pores and octagonal hydrophobic pores (Figure S4). The nature and size of pores accounts for formulae uncertainties, indeed some NH_3 and H_2O molecules were not found from ΔF map (Figures S4 and S7). The confined assemblies are finely stabilized by interactions with the MOF network, which, due to their flexibility, *adapts* pores, in terms of shape (see crystallographic section in Supporting Information for structure refinement details) in relation to the nature of the linker of the cages.

Figure 3 shows that the $[Pd^{II}_6(\mu$–$HOAc)_2(H_2O)_{12}(L_3)_4]$ cages are self–assembled within the confined spaces of **4**, resulting from the reaction of half of the Pd^{2+} ions, from the mononuclear and dinuclear entities stabilized by the precursor (**1**), with the perfluorinated ligand. The templating action of the MOF is undersigned with the final polygon shape, which follows pore's distortion, exhibiting an elliptic geometry. The corners of the $[Pd^{II}_6(\mu$–$HOAc)_2(H_2O)_{12}(L_3)_4]$ cages can be located on $[Pd^{II}_2(\mu$–$HOAc)(H_2O)_2]$ dimeric fragments, which reside at the sides of the elliptic assembly (Figures S2–S3) and interact with the MOF by

means of water–mediated H–bonds. Each Pd(II) exhibits regular square planar geometry, with Pd–N [2.13(2) and 2.077(11) Å for Pd–N_{L3} and 2.070(10) Å for detected Pd–NH_3, respectively], Pd–OH_2 [2.35(2) and 2.30(2) Å for detected Pd–OH_2] and Pd–OAc [2.34(2) Å] bond distances similar, or longer for the latter, to those found in the literature.[74] Figure 3c shows that Pd(II) separations through AcOH and L_3 bridges are 6.96(1) and 13.63(1) Å, respectively. Elliptic polygons are regularly pillared along *c* crystallographic axes, with a Pd(II)···Pd(II) separation among adjacent polygons of 14.94(1) Å (Figure S3 and S5b). Figure 3b shows that the polygons are well–stabilized by mechanical–bonds with the walls of the net, involving terminal H_2O molecules and oxamate residues belonging to the porous network [H_2O···$O_{oxamate}$ of 2.88(1) and 3.27(1) Å] (Figures S3 and S5). Figure 3b also shows that further stabilization is ensured by interactions involving terminal water molecules coordinated to copper metal ions of the network [H–OH···O_{water} 3.15(1) Å] (Figure S3c). The synergic stabilizations, ensured by a such MOF, allow the framework to act as impeccable platform to efficiently safeguard the robustness of the assembled cages, which in turn exhibit high activity in heterogeneous metal–based supramolecular catalysis (*vide infra*). Furthermore, it is worth to note that their size and shape, stabilized near to the walls of the hosting matrix, preserve the available nano–confined spaces, needed for reactants access (Figure S2 and S3a–d).

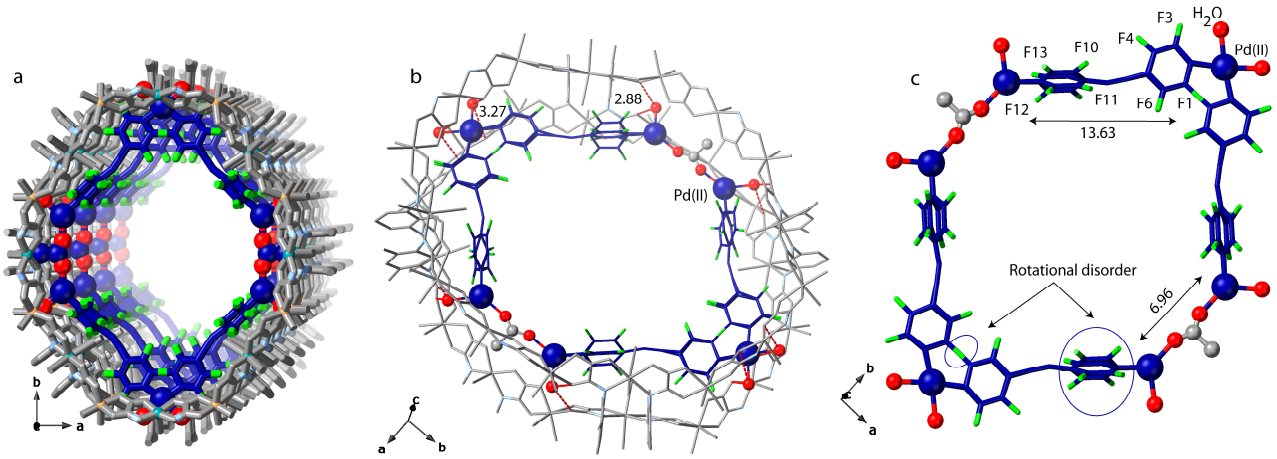

Figure 3. Details of a single pore in crystal structure of 4. Perspective views of a portion of single pores along the [001] direction showing the [Pd^{II}_6(μ–HOAc)$_2$(H_2O)$_{12}$(L_3)$_4$] cages (a) and (b) cages stabilized within MOF's pores by symmetric OH_2 ···O interactions. (c) View of the structure of the cages and related structural parameters. The heterobimetallic $Ni^{II}_4Cu^{II}_6$ 3D anionic network is depicted as grey sticks. Pd(II) cations in the pores and ligands forming the cages, are represented by blue spheres and blue sticks (with fluorine in green), respectively, with oxygen atoms as red spheres. Hydrogen–bonds are represented as red dashed lines.

The experimental PXRD pattern of **4** is identical to the corresponding calculated one (Figure S8). This confirms the homogeneity of the bulk sample, which is isostructural to the crystal selected for single crystal X–ray diffraction. **2** and **3** showed isostructural experimental diffractograms to **4**, which evidenced the similarities of these SCCs@MOF with the crystallographically resolved one. Metal analyses was performed by combined ICP–MS and SEM/EDX measurements (Table S2). The solvent contents of **2**–**4** were determined by TGA under a dry N_2 atmosphere and compared with pristine MOF **1** (Figure S9). All four materials showed a fast mass loss from room temperature, being lower for **2**–**4** than in **1**, which agree with the fact that the cavities of these materials are partially occupied by the *in–situ* constructed SCCs. Then, there is a pseudo plateau until decomposition starts in **1**–**4**. The observed weight losses were 25.72 (**1**), 13.96 (**2**), 14.65 (**3**) and 15.45% (**4**), respectively, and correspond to 52, 25, 26 and 28 water molecules, respectively, which is in line with CHN analyses. N_2 adsorption isotherms of **2**–**4** at 77 K (Figure S10) are also consistent with the decrease in channels accessible void space as consequence of the formation of SCCs@MOF, which agrees with TGA and the crystal structure. Besides, the amount adsorbed is similar to the related non–fluorinated SCCs@MOF previously reported.[71]

XPS evidences a very slight shift of the Pd $3d_{5/2}$ peak of the Pd^{II} atoms in **2**–**4** (338.8, 338.9 and 338.8 eV, respectively) respect **1** (338.6 eV), as it was expected by the low coordination of fluorinated $L_{1–3}$ ligands (Figure S11). XANES results confirm the electrophilicity of Pd^{II} in **2**, similar to **1** without any ligand (Figure S12). EXAFS results for **2** strongly support the formation of the SCCs inside the MOF, with coordination numbers (CN) and estimated distances (Å) for oxygen atoms (CN: 2.35±0.93 and 2.02 Å), nitrogen atoms (CN: 4.40±0.73 and 2.19 Å) and fluorine atoms (CN: 1.50±0.86 and 2.45 Å) in good agreement with the SC–XRD of **4** (Figure S13 and Table S3). Combined liquid NMR and SS MAS ^{19}F–NMR confirmed the complexation to the Pd^{II} site of the perfluorinated ligand L_1 within the SCCs@MOF **2**, since the expected downshift of the signal of free L_1 from ~-126 to ~-118 ppm when complexed to the metal, can be seen, beyond the presence of an impurity coming from the starting material (Figure S14).

These results, together, allowed us to have solid fundaments to establish formulae for **2** and **3** and to further

confirm the results obtained with SCXRD for **4**, as well as give us tools to follow the catalytic experiments within SCCs@MOFs.

2.2. Catalytic experiments

Figure 4a shows the results for the aerobic oxidation of hexanol **5a** to caproic acid **6a** with $Pd(OAc)_2$/2-fluoro-pyridine (^{2}F-py)[30] as a catalyst and different solvents, atmospheres and pressures. The best results were obtained with dioxane as a solvent under 4 bars of O_2 (48.9% yield with >97% selectivity, entry 5). The intermediate aldehyde **7a** was barely detected at the end of the reaction under these conditions and, remarkably, the addition of NaOAc, a typical base for this reaction, does not significantly change neither the yield nor selectivity to **6a** (entry 11), in accordance with the potential ability of Pd^{2+} to catalyze the whole process without base assistance. The lack of base does not adversely affect the reaction progress, since the formed acid does not apparently poison the catalytic system and can be easily isolated after chromatographic separation. The N:Pd ratio in the MOF analyses, corresponding to the expected pyridine to Pd site stoichiometry, excludes the action of any excess of pyridine ligands as a base, which in any case would correspond to an amount of base marginal to improve the catalytic reaction.The formation of high–valence Pd complexes can be excluded on the basis of oxidation experiments with *m*–chloroperbenzoic acid (MCPBA), which do not show any increase in the oxidation yield (entry 8), and control experiments also exclude any role of water during reaction (entry 9). The reaction yield is proportional to the pressure of O_2 (compare entries 10–12). Thus, air can replace pure O_2 as an oxidant, provided that the right partial pressure of O_2 is set, otherwise the oxidation tends to stop in the intermediate aldehyde **7a**. Notice that the oxidation reaction does not evolve without O_2, which discards acceptorless dehydrogenative mechanisms.

Entry	Solvent	Additive	Atmosphere	TON	
				6a	7a
1	-*	-	O_2 (4atm)	0.2	0.2
2	toluene	-	O_2 (4atm)	8.6	n.d.
3	dodecane	-	O_2 (4atm)	5.6	0.4
4	THF	-	O_2 (4atm)	4.2	4.2
5	dioxane	-	O_2 (4atm)	48.9	0.8
6	butyric anhydride	-	O_2 (4atm)	n.d.	0.3
7	dioxane	NaOAc	O_2 (4atm)	57.0	2.2
8	dioxane	MCPBA	O_2 (4atm)	43.0	1.5
9	dioxane	H_2O	O_2 (4atm)	55.8	1.1
10	dioxane	-	N_2 (4atm)	2.1	3.3
11	dioxane	-	reflux	9.4	10.6
12	dioxane	-	air (4atm)	10.1	6.9

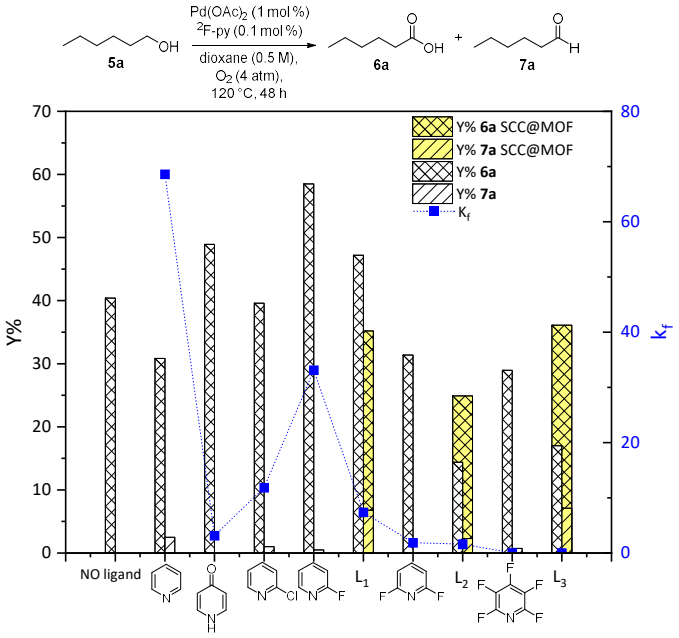

Figure 4. (a) Aerobic oxidation of hexanol **5a** to caproic acid **6a** with $Pd(OAc)_2$/^{2}F–py catalyst under different reaction conditions. Turnover number (TON) equals yield in this case (1 mol% catalyst). (b) Correlation between catalytic activity, pyridine σ electron donation and complex stability for different pyridine–Pd^{2+} complex catalysts. The yields obtained are correlated with the pK_a value of the ligand, which constitutes a valid estimation of the σ electron donation to the Pd^{2+} atom, and the constant of formation for each complex in solution (k_f, square points). Reaction conditions: **5a** 0.25 mmol; [Pd] 1% mol; [pyridine ligand] 0.1% mol; dioxane 0.5M; 120 °C; 48 h; O_2 4 bar. * No solvent.

Figure 4b shows the results for different pyridine–Pd^{2+} complexes under optimized reaction conditions, including fluorinated linear alkynyl bispyridines (L_1-L_3, see Table S4 for numeric yields). Yields of **6a** can be correlated with the pK_a value of the ligand, which constitutes a valid estimation for the σ electron donation of the pyridine to the Pd^{2+} atom,[31] and the constant of formation for each complex in solution, calculated by ^{1}H– and ^{19}F–NMR measurements of each complex (Figures S15–S17, see also catalytic procedures). These correlations show that the catalytic activity increases linearly with the electron donor weakness of the pyridine ligand, reaching a maximum for ^{2}F–py, in accordance with previous reports for other reactions.[1,7] This volcano–type is explained by the lack of formation of the Pd^{2+}–pyridine complex beyond the monofluorinated pyridine, which is confirmed here by the formation constants of the different complexes, drastically decreasing for perfluorinated pyridines (blue squares). Notice that the relationship between k_f for electron-poor pyridines and catalytic activity is qualitative, just to confirm that the formation of the palladium complex is directly related to the catalytic activity, but not quantitative, and the better formation of the MOF-supported fluoropyridine Pd complexes is not assessed here with k_fs. The blank experiment without any

ligand also gives a significant amount of oxidation product, since acetates are relatively low–coordinating ligands, however, a lower amount of oxidation products are found that for many of the electron poor ligands. It must be noticed that the formation of the corresponding fluorobispyridine–Pd^{2+} cages in solution did not occur under standard synthetic conditions for the non–fluorinated cage,[75] which contrast with their formation within MOFs channels (see above). Kinetic experiments with different amounts of NaOAc confirmed that the absence of NaOAc is beneficial for the formation of **6a** (Figure S18).

The catalytic results for the oxidation of **5a** to **6a** with the different MOFs **2**–**4** can also be found in Figure 4b. It can be seen that, in contrast to the corresponding fluoro-pyridine–Pd^{2+} complexes in solution, the yield of **6a** is kept to a maximum value with the perfluorinated cage in MOF **4**. Here, the catalytic activity is defined by a subtle balance between the number of F atoms in the pyridine ligand (electronic effect) and the associated limited diffusion within the microporous framework (steric and coordinating impediments). Indeed, the position of the F atoms in the pyridine ligand also can play a role, beyond the total number of F substituents. For that reason, 2,3–difluoropyridine and 2,3,5,6–tetrafluoropyridine were additionally tested as ligands in solution and the catalytic results (Figure S19 and Table S4) show that it is difficult to establish a sound relationship between number/position of F atoms on the pyridine ligand and catalytic activity in solution, beyond the rough increase in catalytic activity for F–substituted ligands. The formation of the cage is paramount for the catalytic activity within the MOF, since the combination of the ancestor MOF **1**,[73] with bare Pd^{2+} sites, and different soluble pyridine ligands, only catalyze properly the oxidation of **5a** when the appropriate ligand for cage formation is employed (Table S5). The catalytic results with SCC@MOFs **2**–**4** do not exceed the soluble monofluorobipyridine–Pd^{2+} complex, however, they reflect the higher activity of the perfluorinated ligand when forming SCCs@MOF. Also, it will showcase the advantages of translating unrecoverable homogenous catalysts into nanoparticulated recoverable solid catalysts (see below).[76–82]

Figure 5a shows the aerobic oxidation of different aliphatic alcohols of increasing chain length **5a**–**h** catalyzed by SCCs@MOF **4**, under optimized conditions (for numeric values see Table S6). It can be seen that ~30% and ~20% yields, in average, are obtained for <8 atom carbon acids **6a**–**d** and >8 atom carbon acids **6e**–**h**, respectively. These results are in accordance with the channels topology and dimensions (~0.8 nm) of SCCs@MOF **4**, which allows the better diffusion of small linear alkyl chain reactants and products not only through the MOF channels but also through the cages, and complicates the traffic of longer chain molecules. The aerobic oxidation of alkyl alcohols to carboxylic acids is plagued with multiple by-reactions such as ester or ether formation and decarboxylation, and moreover, the absence of base provokes the acidification of the reaction medium, which could trigger more undesired reactions. Thus, the final reaction yields obtanied here with a MOF solid catalyst can be considered reasonable. Figure 5b shows the hot filtration test for SCCs@MOF **4**, which excludes the presence of catalytically active species in solution, and Figure 5c shows that SCCs@MOF **4** keeps its catalytic activity throughout different reuses. PXRD analysis of the fresh and spent solid catalyst confirmed the integrity of the structure (Figure S20). It seems that the catalyst becomes more selective after the first use, nevertheless notice that the yield for **6a** is <10% and **6a** is a potential intermediate of **7a**, thus some variability in the final yield of **6a** may be expected. This variability could come, for instance, from different O_2 pressure during the reuses or slightly modifications of the solid catalyst material during reaction. However, it should be considered that the yields are 35, 45 and 42% for the three reuses, respectively, and a 7% by-product is found in the first use, and none in the second two uses. Thus, the variability for both yield and selectivity is <10% overall, thus it is a reasonable value for a reused solid catalyst. In addition, we have observed that the results with the catalytic SCCs@MOF **2** are not far from the parent monofluorinated complex in solution (Figure S21). These results showcase a clear practical advantage of the solid SCCs@MOFs respect to the homogeneous soluble counterparts, beyond the electronic effects imparted by the perfluorinated ligand.[83-86]

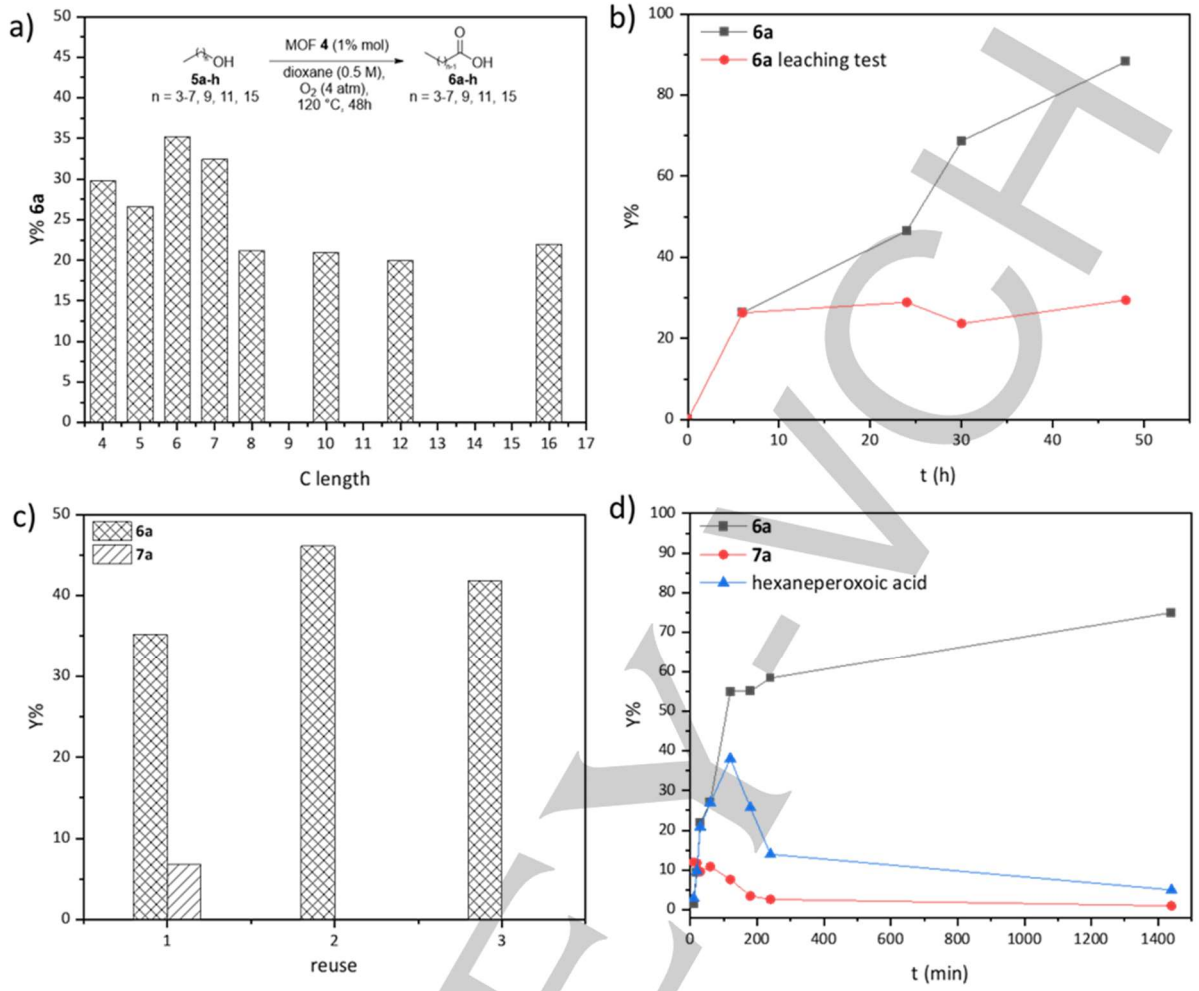

Figure 5 (a) Results for the aerobic oxidation of aliphatic alcohols of increasing chain length catalyzed by solid SCCs@MOF **4**. Selectivity to the carboxylic acid is >97%. Reaction conditions: **5a**–**h** 0.25 mmol; SCCs@MOF **4**, [Pd] 1% mol; dioxane 0.5M; 120 °C; 48 h; O_2 4 bar. (b) and (c) Hot filtration test and reuses of SCCs@MOF **4** for the oxidation of **5a** under optimized conditions. (d) Time dependence for the formation of acid **6a** during the oxidation of intermediate aldehyde **7a**. Reaction conditions: **7a** 0.25 mmol; SCCs@MOF **4**, [Pd] 1% mol; dioxane 0.5M; 120 °C; O_2 4 bar.

Figure 5d shows the kinetics for the oxidation of intermediate hexanal **7a**, catalyzed by SCCs@MOF **4**, under optimized conditions. Each point corresponds to an individual experiment, where O_2 is released and filled back to the reaction to keep the same starting pressure. The formation of caproic acid **6a** perfectly matches with the disappearance of hexanal **7a**, which explains that the intermediate aldehyde is not detected under reaction conditions, since **7a** rapidly oxidizes to **6a** as soon as the former is formed (indeed, the final yield of **6a** is >10% higher when starting from **5a** than **7a**, compare Figures 5b and 5d). These results suggest that the rate–determining step during the oxidation of **5a** to **6a** is the dehydrogenation of **5a** to **7a**. Blank experiments showed that no conversion for any of both reactions occurs if SCCs@MOF **4** is not present (not shown).

Figure 6 shows a plausible mechanism for the oxidation of **5a** to **6a**. Kinetic studies reveal that the rate for the oxidation of hexanol **5a** to caproic acid **6a** follows the equation $r_0 = [\mathbf{5a}][Pd][L]^{-1}$ at low concentrations of **5a** and for any pyridine ligand tested (Figures S22–S27; the error in the data fitting is significant, however, we think that a numerical reaction order can be assigned to, at least, show that the dependence of the reaction rate on the concentration of a particular component is positive, negative or insubstantial). A numerical reaction order O_2 pressure does not appear in the rate equation, in accordance with the rapid oxidation of hexanal **7a** to caproic acid **6a**, and the reaction order for hexanal **7a** matches **5a** under similar reaction conditions, which further confirms the intermediacy and rapid oxidation of **7a** (Figure S28). Besides, [**5a**] has no influence on the reaction rate at concentrations >3:1 respect to [Pd^{2+}], thus when the Pd complex is already saturated by the alcohol (Figure S22). These results strongly suggest that the catalytic species corresponds to a Pd^{2+} complex where the alcohol has replaced the pyridine ligand, to be efficiently dehydrogenated by the electrophilic Pd^{2+} site. This cationic Pd site is now available to receive the hydroperoxy molecule (see ahead). The highly competitive coordination of the pyridine ligand explains why the perfluorinated Pd^{2+} cages in

SCCs@MOFs **2**–**4**, despite having the optimal electronics in the ligands, are only slightly more efficient that the monofluoropyridine–Pd^{2+} complex in solution, since the forced ligand–to–metal interaction in the confined coordination cage must severely impede the coordination of alcohol **5a**. However, the catalytic results obtained by the solid SCCs@MOFs **2**–**4** have to be put in context and remarked, if one considers not only the intrinsic steric and coordination hindrance of the cage but also the lower mobility of the reactants/products inside the micro–structured SCCs@MOFs compared to the open catalytic Pd^{2+} complexes in solution.

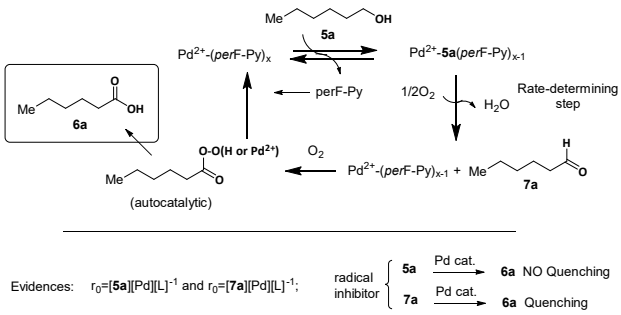

Figure 6 Plausible mechanism for the oxidation of **5a** to **6a**.

Considering that the aldehyde is the undiscussed precursor of the acid, and in order to unveil the rapid oxidation mechanism operating during the reaction, the rate equation and possible transient species during the oxidation of hexanal **7a** to caproic acid **6a** was studied (Figures S29–S34). The results with different fluoropyridine–Pd^{2+} catalysts show that hexanehydroperoxy acid is formed in all cases, and it rapidly collapses into the final acid **6a**, with a rate equation $r_0 = [\mathbf{7a}][Pd][L]^{-1}$. This rate equation is identical to the direct oxidation process, from hexanol **5a** to caproic acid **6a**. The use of radical inhibitors (Figure S35) quenches the oxidation of aldehyde **7a** to **6a**, and the dehydrogenation of alcohol **5a** to **7a**. These results strongly support alkylhydroperoxy acids as intermediates during the oxidation of the aldehyde, which are accepted intermediates during the autocatalyzed oxidation of aldehydes to carboxylic acids.[87] These peroxy acids join the potential formation of explosive peroxide intermediates with solvent dioxane under O_2, which probably makes the system unsuitable at the industrial level but certainly promising and worthy of further exploration.

Conclusions

SCCs of Pd^{2+} with (per)fluorinated pyridines are formed within the channels of an anionic tridimensional MOF and are able to catalyse the aerobic oxidation of alkyl alcohols to carboxylic acids without assistance of any additive/base. Related SCCs supported on MOFs but without (per)fluorinated pyridine ligands are not able to efficiently perform such transformation.[71] The structure of these new solid materials was determined by a multi–technique approach including single-crystal X-ray crystallography, allowing to unveiled how reticular chemistry and supramolecular chemistry are connecting in the task to produce highly stable and well-performing materials. These recoverable solid materials not only expand the Pd organometallic chemistry towards stable, extremely high electrophilic Pd^{2+} sites, but also open the door to their use as catalysts in challenging C–H activation reactions.

Acknowledgements

This work was supported by the Ministero dell'Istruzione, dell'Università e della Ricerca (Italy), the MICINN (Spain) (Projects PID2019−104778GB−I00, 2017–86735–P, PID2020-115100GB-I00, and Excellence Units "Severo Ochoa" and "Maria de Maeztu" SEV–2016–0683 and CEX2019−000919−M) and the Engineering and Physical Sciences Research Council (UK). The work has also been funded by Generalitat Valenciana, Prometeo Grupos de Investigación de Excelencia (PROMETEU/2021/054). R.G. thanks ITQ for a contract. J.O.–M. acknowledges the Juan de la Cierva program for the concession of a contract (IJC2018–036514–I). D.A. acknowledges the financial support of the Fondazione CARIPLO / "Economia Circolare: ricerca per un futuro sostenibile" 2019, Project code: 2019–2090, MOCA and Diamond Light Source for awarded beamtime and provision of synchrotron radiation facilities and thank Dr David Allan and Sarah Barnett for their assistance at I19 beamline (Proposal No. CY22411-1). Thanks are also extended to the 2019 Post–doctoral Junior Leader–Retaining Fellowship, la Caixa Foundation (ID100010434 and fellowship code LCF/BQ/PR19/11700011), the "Generalitat Valenciana" (SEJI/2020/034) and the "Ramón y Cajal" program (J.F.–S.). E.P. acknowledges the financial support of the European Research Council under the European Union's Horizon 2020 research and innovation programme / ERC Grant Agreement No 814804, MOF–reactors. E. T-F thanks the MICINN for a PhD FPI grant.

Keywords: per–fluorinated palladium complexes • metal-organic frameworks • supramolecular coordination cages • aerobic alcohol oxidation to carboxylic acid • single crystal X–Ray diffraction

[1] D. Zhao, P. Xu, T. Ritter, *Chem* **2019**, *5*, 97–107.

[2] C. A. Salazar, K. N. Flesch, B. E. Haines, P. S. Zhou, D. G. Musaev, S. S. Stahl, *Science* **2020**, *370*, 1454–1460.

[3] J. Vercammen, M. Bocus, S. Neale, A. Bugaev, P. Tomkins, J. Hajek, S. Van Minnebruggen, A. Soldatov, A. Krajnc, G. Mali, et al., *Nat. Catal.* **2020**, *3*, 1002–1009.

[4] G. t. Brink, *Science* **2000**, *287*, 1636–1639.

[5] D. L. Bruns, D. G. Musaev, S. S. Stahl, *J. Am. Chem. Soc.* **2020**, *142*, 19678–19688.

[6] D. C. Powers, E. Lee, A. Ariafard, M. S. Sanford, B. F. Yates, A. J. Canty, T. Ritter, *J. Am. Chem. Soc.* **2012**, *134*, 12002–12009.

[7] C. C. Roberts, E. Chong, J. W. Kampf, A. J. Canty, A. Ariafard, M. S. Sanford, *J. Am. Chem. Soc.* **2019**, *141*, 19513–19520.

[8] J. A. Tunge, L. N. Foresee, *Organometallics* **2005**, *24*, 6440–6444.

[9] K. Li, Y. Zeng, B. Neuenswander, J. A. Tunge, *J. Org. Chem.* **2005**, *70*, 6515–6518.

[10] J. K. Kirsch, J. L. Manske, J. P. Wolfe, *J. Org. Chem.* **2018**, *83*, 13568–13573.

[11] N. Lebrasseur, I. Larrosa, *J. Am. Chem. Soc.* **2008**, *130*, 2926–2927.

[12] R. Kudirka, S. K. J. Devine, C. S. Adams, D. L. Van Vranken, *Angew. Chem. Int. Ed.* **2009**, *48*, 3677–3680.

[13] M. S. Sigman, E. W. Werner, *Acc. Chem. Res.* **2012**, *45*, 874–884.

[14] Z. She, Y. Shi, Y. Huang, Y. Cheng, F. Song, J. You, *Chem. Commun.* **2014**, *50*, 13914–13916.

[15] A. C. Kruegel, S. Rakshit, X. Li, D. Sames, *J. Org. Chem.* **2015**, *80*, 2062–2071.

[16] J. R. Cabrero-Antonino, M. Tejeda-Serrano, M. Quesada, J. A. Vidal-Moya, A. Leyva-Pérez, A. Corma, *Chem. Sci.* **2017**, *8*, 689–696.

[17] T. U. Thikekar, C.-M. Sun, *Adv. Synth. Catal.* **2017**, *359*, 3388–3396.

[18] H. T. Kim, W. Lee, E. Kim, J. M. Joo, *Chem. Asian J.* **2018**, *13*, 2418–2422.

[19] T. Korenaga, R. Sasaki, K. Shimada, *Dalt. Trans.* **2015**, *44*, 19642–19650.

[20] Y. Izawa, S. S. Stahl, *Adv. Synth. Catal.* **2010**, *352*, 3223–3229.

[21] L. I. Panferova, M. O. Zubkov, V. A. Kokorekin, V. V. Levin, A. D. Dilman, *Angew. Chem. Int. Ed.* **2021**, *60*, 2849–2854.

[22] R. P. Singh, G. V. Eggers, J. M. Shreeve, *Synthesis* **2003**, *2003*, 1009–1011.

[23] K. L. Hull, W. Q. Anani, M. S. Sanford, *J. Am. Chem. Soc.* **2006**, *128*, 7134–7135.

[24] F. Du, Q. Zhou, D. Liu, T. Fang, Y. Shi, Y. Du, G. Chen, *Synlett* **2018**, *29*, 779–784.

[25] G. S. Biggs, M. J. O'Neill, P. Carames Mendez, T. G. Scrase, Y. Lin, A. M. Bin-Maarof, A. D. Bond, S. R. Boss, P. D. Barker, *Dalt. Trans.* **2019**, *48*, 6910–6920.

[26] Y. Y. See, M. T. Morales-Colón, D. C. Bland, M. S. Sanford, *Acc. Chem. Res.* **2020**, *53*, 2372–2383.

[27] I. Klemet, H. Lütjens, P. Knochel, *Angew. Chem. Int. Ed.* **1997**, *36*, 1454–1456.

[28] R. Boyaala, M. Peng, W.-S. Tai, R. Touzani, T. Roisnel, V. Dorcet, Y. Chi, V. Guerchais, H. Doucet, J.-F. Soulé, *Inorg. Chem.* **2020**, *59*, 13898–13911.

[29] A. Sen, M. Lin, *Direct Catalytic Oxidative Carbonylation of Lower Alkanes to Acids (US08/357,437)*, **1996**.

[30] R. . Sheldon, I. W. C. . Arends, A. Dijksman, *Catal. Today* **2000**, *57*, 157–166.

[31] K. Noweck, W. Grafahrend, in *Ullmann's Encycl. Ind. Chem.*, Wiley-VCH Verlag GmbH & Co. KGaA, Weinheim, Germany, **2006**.

[32] V. Cherepakhin, T. J. Williams, *Synthesis* **2021**, *53*, 1023–1034.

[33] R. K. Sodhi, S. Paul, J. H. Clark, *Green Chem.* **2012**, *14*, 1649.

[34] T. Mallat, A. Baiker, *Catal. Today* **1994**, *19*, 247–283.

[35] S. Mannam, G. Sekar, *Synth. Commun.* **2010**, *40*, 2822–2829.

[36] Q. Gu, W.-H. Fang, R. Wischert, W.-J. Zhou, C. Michel, M. Pera-Titus, *J. Catal.* **2019**, *380*, 132–144.

[37] J. Sha, E.-J. Zheng, W.-J. Zhou, A. Liebens, M. Pera-Titus, *J. Catal.* **2016**, *337*, 199–207.

[38] B. Mahmoudi, A. Rostami, M. Kazemnejadi, B. A. Hamah-Ameen, *Green Chem.* **2020**, *22*, 6600–6613.

[39] X. Jiang, J. Zhang, S. Ma, *J. Am. Chem. Soc.* **2016**, *138*, 8344–8347.

[40] M. Zhao, X.-W. Zhang, C.-D. Wu, *ACS Catal.* **2017**, *7*, 6573–6580.

[41] H.-M. Liu, L. Jian, C. Li, C.-C. Zhang, H.-Y. Fu, X.-L. Zheng, H. Chen, R.-X. Li, *J. Org. Chem.* **2019**, *84*, 9151–9160.

[42] G.-J. ten Brink, I. W. C. E. Arends, R. A. Sheldon, *Adv. Synth. Catal.* **2002**, *344*, 355–369.

[43] M. J. Schultz, C. C. Park, M. S. Sigman, *Chem. Commun.* **2002**, 3034–3035.

[44] D. R. Jensen, M. J. Schultz, J. A. Mueller, M. S. Sigman, *Angew. Chem. Int. Ed.* **2003**, *42*, 3810–3813.

[45] M. Yang, K.-T. Yip, J.-H. Pan, Y.-C. Chen, N.-Y. Zhu, D. Yang, *Synlett* **2006**, *18*, 3057–3060.

[46] S. Gowrisankar, H. Neumann, D. Gördes, K. Thurow, H. Jiao, M. Beller, *Chem. Eur. J.* **2013**, *19*, 15979–15984.

[47] Y. Uozumi, R. Nakao, *Angew. Chem. Int. Ed.* **2003**, *42*, 194–197.

[48] D. Wang, J. N. Jaworski, S. S. Stahl, in *Liq. Phase Aerob. Oxid. Catal. Ind. Appl. Acad. Perspect.*, Wiley-VCH Verlag GmbH & Co. KGaA, Weinheim, Germany, **2016**, pp. 113–138.

[49] B. Karimi, S. Abedi, J. H. Clark, V. Budarin, *Angew. Chem. Int. Ed.* **2006**, *45*, 4776–4779.

[50] Z. Hou, N. Theyssen, W. Leitner, *Green Chem.* **2007**, *9*, 127–132.

[51] K. Mori, T. Hara, T. Mizugaki, K. Ebitani, K. Kaneda, *J. Am. Chem. Soc.* **2004**, *126*, 10657–10666.

[52] W. Hou, N. Dehm, R. Scott, *J. Catal.* **2008**, *253*, 22–27.

[53] M. Rafiee, Z. M. Konz, M. D. Graaf, H. F. Koolman, S. S. Stahl, *ACS Catal.* **2018**, *8*, 6738–6744.

[54] E. Tiburcio, R. Greco, M. Mon, J. Ballesteros-Soberanas, J. Ferrando-Soria, M. López-Haro, J. C. Hernández-Garrido, J. Oliver-Meseguer, C. Marini, M. Boronat, et al., *J. Am. Chem. Soc.* **2021**, *143*, 2581–2592.

[55] T. Wang, C.-X. Xiao, L. Yan, L. Xu, J. Luo, H. Shou, Y. Kou, H. Liu, *Chem. Commun.* **2007**, 4375.

[56] T. Wang, H. Shou, Y. Kou, H. Liu, *Green Chem.* **2009**, *11*, 562.

[57] J. A. Mueller, C. P. Goller, M. S. Sigman, *J. Am. Chem. Soc.* **2004**, *126*, 9724–9734.

[58] M. J. Schultz, R. S. Adler, W. Zierkiewicz, T. Privalov, M. S. Sigman, *J. Am. Chem. Soc.* **2005**, *127*, 8499–8507.

[59] M. Mon, R. Adam, J. Ferrando−Soria, A. Corma, D. Armentano, E. Pardo, A. Leyva−Pérez, *ACS Catal.* **2018**, *8*, 10401–10406.

[60] N. Riemer, M. Shipman, P. Wessig, B. Schmidt, *J. Org. Chem.* **2019**, *84*, 5732–5746.

[61] S. Ishikawa, N. Noda, M. Wada, S. Tsurumi, W. Ueda, *ACS Catal.* **2020**, *10*, 10535–10545.

[62] J. M. Hoover, S. S. Stahl, *J. Am. Chem. Soc.* **2011**, *133*, 16901–16910.

[63] D. Kong, P. J. Moon, E. K. J. Lui, O. Bsharat, R. J. Lundgren, *Science* **2020**, *369*, 557–561.

[64] H.-C. Zhou, J. R. Long, O. M. Yaghi, *Chem. Rev.* **2012**, *112*, 673–674.

[65] N. Stock, S. Biswas, *Chem. Rev.* **2012**, *112*, 933–969.

[66] H. Furukawa, K. E. Cordova, M. O'Keeffe, O. M. Yaghi, *Science* **2013**, *341*, 974.

[67] H.-C. Zhou, S. Kitagawa, *Chem. Soc. Rev.* **2014**, *43*, 5415–5418.

[68] Y. Cui, B. Li, H. He, W. Zhou, B. Chen, G. Qian, *Acc. Chem. Res.*

2016, *49*, 483–493.

[69] A. Kirchon, L. Feng, H. F. Drake, E. A. Joseph, H.-C. Zhou, *Chem. Soc. Rev.* **2018**, *47*, 8611–8638.

[70] G. Maurin, C. Serre, A. Cooper, G. Férey, *Chem. Soc. Rev.* **2017**, *46*, 3104–3107.

[71] R. Adam, M. Mon, R. Greco, L. H. G. Kalinke, A. Vidal-Moya, A. Fernandez, R. E. P. Winpenny, A. Doménech-Carbó, A. Leyva-Pérez, D. Armentano, et al., *J. Am. Chem. Soc.* **2019**, *141*, 10350–10360.

[72] B. Li, Y. Zhang, D. Ma, T. Ma, Z. Shi, S. Ma, *J. Am. Chem. Soc.* **2014**, *136*, 1202–1205.

[73] F. R. Fortea-Pérez, M. Mon, J. Ferrando-Soria, M. Boronat, A. Leyva-Pérez, A. Corma, J. M. Herrera, D. Osadchii, J. Gascon, D. Armentano, et al., *Nat. Mater.* **2017**, *16*, 760–766.

[74] J.-H. Chu, Z.-H. Su, K.-W. Yen, H.-I. Chien, *Organometallics* **2020**, *39*, 3168–3179.

[75] M. Fujita, O. Sasaki, T. Mitsuhashi, T. Fujita, J. Yazaki, K. Yamaguchi, K. Ogura, *Chem. Commun.* **1996**, 1535.

[76] S. Mitchell, R. Qin, N. Zheng, J. Pérez-Ramírez, *Nat. Nanotechnol.* **2021**, *16*, 129–139.

[77] A. Abad, P. Concepción, A. Corma, H. García, *Angew. Chem. Int. Ed.* **2005**, *44*, 4066–4069.

[78] A. Abad, C. Almela, A. Corma, H. García, *Tetrahedron* **2006**, *62*, 6666–6672.

[79] D. I. Enache, J. K. Edwards, P. Landon, B. Solsona-Espriu, A. F. Carley, A. A. Herzing, M. Watanabe, C. J. Kiely, D. W. Knight, G. J. Hutchings, *Science* **2006**, *311*, 362–365.

[80] B. Karimi, F. Mansouri, H. Vali, *ACS Appl. Nano Mater.* **2020**, *3*, 10612–10627.

[81] B. A. Steinhoff, S. R. Fix, S. S. Stahl, *J. Am. Chem. Soc.* **2002**, *124*, 766–767.

[82] B. A. Steinhoff, S. S. Stahl, *J. Am. Chem. Soc.* **2006**, *128*, 4348–4355.

[83] A. Dhakshinamoorthy, H. Garcia, *ChemSusChem* **2014**, *7*, 2392–2410.

[84] A. Dhakshinamoorthy, A. M. Asiri, H. Garcia, *Chem. Commun.* **2017**, *53*, 10851–10869.

[85] A. Dhakshinamoorthy, A. M. Asiri, H. Garcia, *Trends Chem.* **2020**, *2*, 454–466.

[86] A. Dhakshinamoorthy, A. M. Asiri, H. Garcia, *ChemCatChem* **2020**, *12*, 4732–4753.

[87] M. Sankar, E. Nowicka, E. Carter, D. M. Murphy, D. W. Knight, D. Bethell, G. J. Hutchings, *Nat. Commun.* **2014**, *5*, 3332.

Entry for the Table of Contents

COMMUNICATION

Fluorinated pyridine–Pd^{2+} coordinate cages have been synthesized and characterized with atomic resolution within the channels of a metal organic framework (MOF), and used as catalysts during the aerobic oxidation of aliphatic alcohols to carboxylic acids without any additive. These results illustrate a rare example of stable per–fluorinated cationic metal complex, with potential implications in the future design of catalytic organometallic complexes.

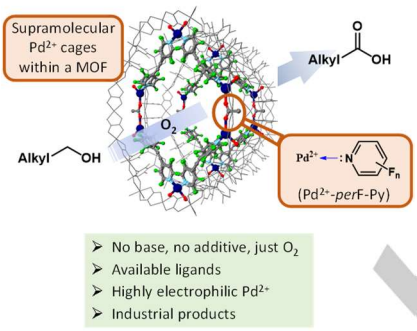

Rossella Greco, Estefania Tiburcio–Fortes, Antonio Fernandez, Carlo Marini, Alejandro Vidal–Moya, Judit Oliver–Meseguer, Donatella Armentano, Emilio Pardo,* Jesús Ferrando–Soria,* Antonio Leyva–Pérez.**

Page No. – Page No.

MOF–stabilized perfluorinated palladium cages catalyze the additive–free aerobic oxidation of aliphatic alcohols to acids